Accepted Manuscript. The final article was published in: Dalton Trans., 2017,46, 9227-9234 and is available at: https://doi.org/10.1039/C7DT02165H

Journal Name

ARTICLE

Synthesis, Structure and Dispersion Interactions in Bis(1,8-naphthalendiyl)distibine

Received 00th January 20xx,

Accepted 00th January 20xx

DOI: 10.1039/x0xx00000x

www.rsc.org/

C. Ganesamoorthy,[a] S. Heimann,[a] S. Hölscher,[a] R. Haack,[a] C. Wölper,[a] G. Jansen*[,a] and S. Schulz*[,a,b]

Abstract. $Naph_2Sb_2$ **1** was synthesized by reaction of 1,8-dilithionaphthalene $NaphLi_2$ with $SbCl_3$ and its solid state structure is reported. **1** shows intermolecular interactions in the solid state, which were studied by quantum chemical calculations with dispersion corrected density functional theory, supermolecular *ab initio* approaches and symmetry adapted perturbation theory. The same methods were employed to compare the solid state interactions in the crystal of **1** to those in real (for E=P) and hypothetical (for E= As and Bi) crystal structures of $Naph_2E_2$. Dispersion interactions were found to provide the most important stabilising contribution in all cases, seconded by electrostatic attraction between pnictogen atoms and π-systems of neighbouring naphthyl groups.

Introduction

Divalent group 15 compounds $R_2E\text{-}ER_2$ (E = P, As, Sb, Bi) containing a central E-E bond are well known compounds. Me_4As_2 ("*fuming arsenical liquid*" or "*Cacodyl*") represents the first organometallic compound and was initially prepared by Louis Cadet de Gassicourt in 1760 and later on investigated by Robert Bunsen.[1] The heavier group 15 homologues, Me_4Sb_2 and Me_4Bi_2 were prepared in the early 1930's,[2] but systematic studies on the synthesis, structure and reactivity of such compounds were not started before the early 1980's.[3] Moreover, the thermochromic behaviour, which refers to the colour change observed for some distibines and dibismuthines upon melting/freezing,[2,4] was investigated and found to originate from intermolecular metal···metal interactions in the solid state.[5] Distibines and dibismuthines were found to easily undergo homolytic bond cleavage reactions due to the rather weak Sb-Sb and Bi-Bi bonds,[6] but persistent Sb- and Bi-centred radicals have only been recently observed.[7]

Our interest in the solid state structures and intermolecular interactions in R_4E_2 (E = Sb, Bi)[8,9] prompted our attention to a distibine with a rigid ligand backbone. The 1,8-naphtalendiyl ligand (Naph) is a promising ligand due to its capability to stabilize group 15 elements,[10] i.e. 1,8-$(R_2Sb)_2$Naph,[11] chalcogen-[12] and P/chalcogen-substituted compounds.[13,14] We now report on the synthesis of $Naph_2Sb_2$ **1** and the role of dispersion interactions on the solid state structure. To investigate the latter point we employed a variety of quantum chemical methods comprising dispersion corrected density functional theory, supermolecular *ab initio* approaches and symmetry adapted perturbation theory. Furthermore, these methods were also used to study interactions in real (for E=P) and hypothetical (for E= As and Bi) solid state structures of $Naph_2E_2$.

Results and discussion

$Li_2Naph{\cdot}TMEDA$ reacts with $SbCl_3$ in 3:2 molar ratio with LiCl elimination and formation of $Naph_2Sb_2$ **1** in moderate yield (48%). **1** is poorly soluble in benzene, toluene and chloroform. Its ^1H NMR spectrum shows two doublets (8.03, 7.55 ppm) and a triplet (7.34 ppm) and the ^{13}C NMR spectrum shows the expected six singlets for the Naph substituent.

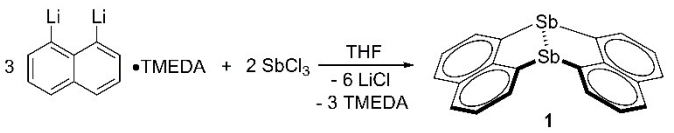

Scheme 1. Synthesis of **1**.

Single crystals of **1** were obtained upon storage of a solution of **1** in $CHCl_3$ at 0 °C for 3 days.[15] **1** crystallises in the triclinic space group *P*-1 with one independent molecule in the asymmetric unit and adopts a butterfly-type structure, in which the Sb-Sb bond is clamped by the naphthalene wings (fig. 1). Each Sb atom shows trigonal-pyramidal coordination sphere with bond angles close to 90° as was expected for non-hybridised p-orbitals. However, the C–Sb–C bond angles are roughly 5° larger and the C–Sb–Sb bond angles 5° smaller than the ideal 90° value, most likely resulting from the shorter distances between the coordinating carbon atoms of the ligands (2.51(3)

[a] *University of Duisburg-Essen, Universitätsstr. 5-7, S07 S03 C30, 45117 Essen, Germany. Fax: Int (+)201 1833830; Tel: Int (+)201 1834635; E-mail: stephan.schulz@uni-due.de; Tel: Int (+)201 1834421; georg.jansen@uni-due.de.*
[b] *Center for Nanointegration Duisburg-Essen(Cenide), University of Duisburg-Essen.*

† Dedicated to Prof. D. Naumann on the occasion of his 75th birthday.

Electronic Supplementary Information (ESI) available: NMR and IR spectra and crystallographic data of **1**; quantum chemical calculations. See DOI: 10.1039/x0xx00000x

CCDC 1537302 (**1**) contains the supplementary crystallographic data for this paper. These data can be obtained free of charge from The Cambridge Crystallographic Data Centre *via* www.ccdc.cam.ac.uk/data_request/cif.

Å) compared to the Sb–Sb bond. The Sb-Sb bond length (2.7972(3) Å) agrees with the sum of the covalent radii (single-bond cov. radius of Sb 1.40 Å) but is shorter than the mean Sb-Sb bond lengths observed in distibines Sb_2R_4 (2.862(2) Å)[16] as a result from the constrained geometry of the molecule.

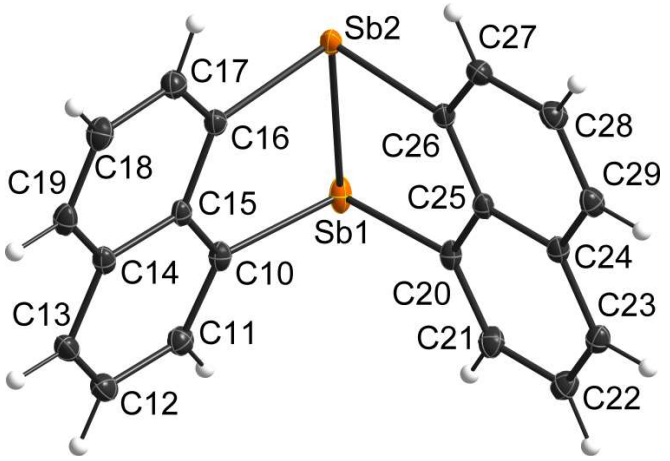

Figure 1. Solid state structure of **1**; non-H-atoms are shown as thermal ellipsoids at 50% probability levels. Selected bond lengths [Å] and angles [°]: Sb(1)-Sb(2) 2.7972(3), Sb(1)-C(10) 2.1602(19), Sb(1)-C(20) 2.1695(18), Sb(2)-C(26) 2.1595(18), Sb(2)-C(16) 2.1658(19), C(10)-Sb(1)-C(20) 95.38(7), C(10)-Sb(1)-Sb(2) 86.33(5), C(20)-Sb(1)-Sb(2) 86.17(5), C(26)-Sb(2)-C(16) 94.25(7), C(26)-Sb(2)-Sb(1) 86.26(5), C(16)-Sb(2)-Sb(1) 86.08(5).

Short Sb-Sb bonds were also observed in paddlewheel-type 1,2,4-diazaphospholid- (2.6691(8)–2.7451(8) Å) and diaza-phosphadistibines (2.64438(4) Å).[17] The five-membered C_3Sb_2 rings and the naphthalene groups in **1**, which are oriented in a perpendicular position and hence show a dihedral angle of 96.95(7)° (C10-Sb1-Sb2-C26 torsion angle) or 85.36(4)° (angle between planes of the ligands), are almost planar. The av. Sb-C bond length in **1** (2.1637(19) Å) is comparable to those reported for 1,8-$(R_2Sb)_2$-$C_{10}H_8$[11] and matches values found in the CSD (1.756 - 2.406 Å, mean 2.136(36) Å). The molecular structure of $Naph_2P_2$, the P-analogue of **1**, is similar to that of **1**.[18] However, the average C-P-C (99.62(7)°) and C-P-P bond angles (93.25(5)°) are larger than the C-Sb-C and C-Sb-Sb angles in **1**, indicating a higher s-character (respectively lower p-character) of the bonding electron pairs in $Naph_2P_2$ compared to **1** as was expected due to the less pronounced tendency of hybridisation for Sb compared to P. Consequently, the bonding electron pairs of **1** mainly consist of p-character. 2,7-diphosphatetracyclo[6.2.2.2^{3,6}.0^{2,7}]tetradeca-4,9-diene[19] and 1,6-diphosphabicyclo(4.4.0)deca-3.8-diene also show larger C-P-C and C-P-P bond angles in the solid state.[20]

Since intermolecular interactions in E_2R_4 (E = Sb, Bi) have been discussed with respect to the thermochromic effect,[5,8] we investigated the solid state structure of **1** in detail. Figure 2 displays the 3D packing of **1** in the solid state, while different types of intermolecular interactions in **1** are shown in Figure 3. **1** shows classical π···π and CH···π contacts, furthermore Sb···π contacts, whereas direct Sb···Sb contacts are missing. The packing of $Naph_2P_2$ is similar but not identical (monoclinic $P2_1/c$) to **1** (Fig. 4).

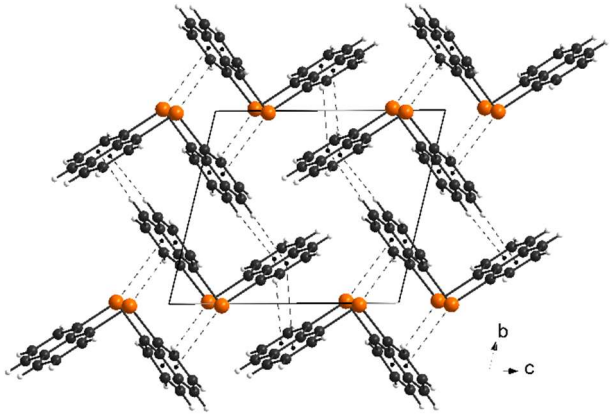

Figure 2. 3D packing plot of **1** in the solid state; non-H-atoms are shown as thermal ellipsoids at 50% probability levels.

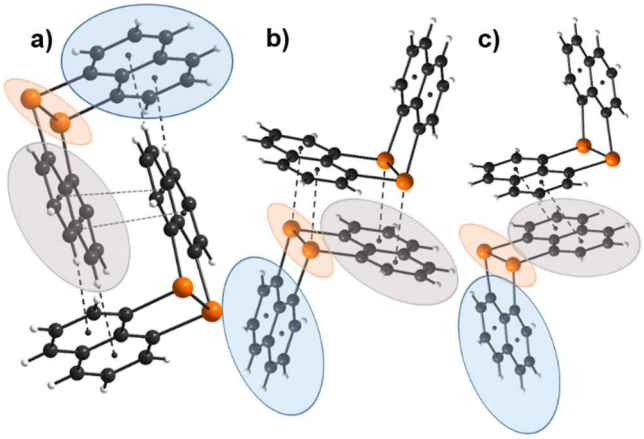

Figure 3. CH···π / π···π (a), Sb···π (b) and π···π (c) interactions in the packing of **1**; fragments ds (orange), np (grey), np' (blue).

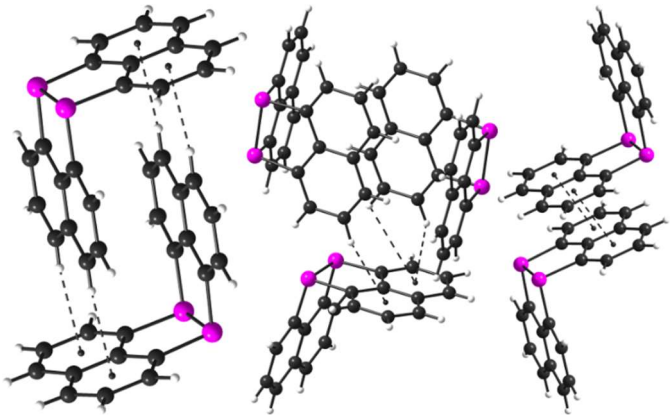

Figure 4. CH···π / π···π (a), CH···π (b) and π···π (c) interactions in the packing of $Naph_2P_2$.

Both compounds show two centrosymmetric motifs (Fig. 3a/3c, Fig. 4a/4c), while a third CH···π contact (Fig. 4b) in $Naph_2P_2$, which is constituted via 2_1 symmetry, cannot appear

in the triclinic structure of **1**. In contrast, a P···π contact (similar to Fig. 3b; replacement of Sb by P) does not exist in $Naph_2P_2$.
We further investigated the bonding situation and intermolecular interactions in **1** by quantum chemical calculations[21] and first investigated, whether the three nearest neighbour structures as observed in the crystal (fig. 3) also represent stable conformers of the dimer *in vacuo*. Geometry optimizations at the BP+D3 level of theory with a triple-zeta (TZ) quality basis set were performed.[22-25]

Table 1. Selected Intra- and Intermolecular distances (in Å) and angles (in °) for nearest neighbour pairs (**1a**, **1b**, **1c)** in the crystal structure and after *in vacuo* geometry optimization of the corresponding dimer (**1a'**, **1b'**, **1c'**) at the BP+D3/TZ level.

	Sb-Sb	C-Sb-C	Sb···Sb	Sb···π	π ···π	CH···π
1a	2.797	94.2/95.4	9.06	8.69/8.61	3.76	2.71/2.77
1a'	2.808	93.2/93.6	9.07	5.87/5.94	3.64	2.41/2.51
1b	2.797	94.2/95.4	4.61	3.65/3.86	5.69	----
1b'	2.806	92.4/92.8	5.13	3.73/3.90	5.35	----
1c	2.797	94.2/95.4	6.52	3.99/4.08	3.94	----
1c'	2.801	93.3/93.4	6.92	4.26/4.30	3.79	----

π refers to the geometrical midpoint of a C_6-ring within the naphthalene unit.

The Sb-Sb distance in the optimized structures **1a'**, **1b'**, **1c'** agrees within 0.01 Å with that of the crystal structure and with the optimized monomer structure (2.808 Å). In contrast, the calculated C-Sb-C bond angles differ noticeably by up to 3° from the crystal structure and are also smaller than the corresponding angle of the monomer (93.7°). Though qualitatively the dimer structures did not much change during geometry optimization, we note a slight parallel slide of the two subunits in **1b**, resulting in longer intermolecular Sb···Sb distances and shorter π···π distances. We observed a similar effect for **1c**, while in **1a** the main effect is a slight shrinking of the long edge of the "brick". **1a** is the most stable nearest neighbour structure with a BP+D3 level interaction energy of -97.1 kJ/mol with respect to dissociation into non-relaxed monomers (monomer structure fixed to that found in the crystal). This nearly coincides with the stabilization energy of -98.7 kJ/mol of **1a'**, measured with respect to dissociation into relaxed monomers. **1c** displays somewhat larger differences between the interaction energy of -65.4 kJ/mol for the crystal structure neighbours and the stabilization energy of -69.6 kJ/mol for the corresponding optimized dimer **1c'**. For the least stable neighbour pair **1b**, the magnitude of the non-relaxed nearest neighbour interaction energy (-58.1 kJ/mol) is significantly smaller than that of the stabilization energy (-64.4 kJ/mol) of the optimized dimer **1b'**. The interactions discussed so far may be viewed as occurring within an infinite layer of bricks **1a** (interactions **1b** and **1c** connecting these bricks). We also determined interactions of nearest neighbour pairs (**1d** and **1e**, see ESI) of *different* layers. With -24.4 and -17.1 kJ/mol, respectively, they are significantly smaller than the intralayer interactions.

Decomposing **1** into fragments (Fig. 3) and capping these with H-atoms allows a more detailed understanding of the important contributors to the nearest neighbours interaction energies. It further allows applying high level quantum chemical methods for the determination of the interaction energy. Starting from the crystal structure of **1** we thus created naphthalene (np, np') and Sb_2H_4 (ds) fragments through replacing Sb-C bonds with Sb-H and C-H bonds, scaling the bond vectors down to magnitudes of 1.72 [26] and 1.09 Å,[27] respectively.

Table 2 shows the fragment-fragment interaction energies as determined from a variety of quantum chemical methods, i.e. besides BP-D3 and PBE-D3[23,28](in which the exchange correlation functional is different and the dispersion correction is readapted accordingly) also counterpoise-corrected (CPC)[29] spin-component-scaled MP2 (SCS-MP2)[30] and symmetry-adapted perturbation theory combined with DFT (DFT-SAPT)[31] with double- (DZ) and triple-zeta (TZ) quality basis sets.[32,25] Counterpoise-corrected single and double excitation coupled-cluster theory including perturbative triple excitations (CCSD(T)), the latter with a double-zeta quality basis set, were applied for reference.

Table 2. Fragment-fragment interaction energies (in kJ/mol).

		ds···np	ds···np'	ds···ds	np···np	np··np'
1a	BP+D3/TZ	-7.19	-0.40	-0.34	-33.21	-24.72
	PBE-D3/TZ	-8.90	-0.36	-0.31	-24.36	-22.01
	CCSD(T)/DZ	-6.80	-0.34	-0.32		
	SCS-MP2/DZ	-6.09	-0.35	-0.30	-24.84	-16.99
	SCS-MP2/TZ	-6.56	-0.38	-0.32	-26.62	-18.09
	DFT-SAPT/DZ	-5.97	-0.32	-0.28	-18.35	-15.72
	DFT-SAPT/TZ	-6.56	-0.32	-0.30	-20.53	-16.71
1b	BP+D3/TZ	-20.26	-1.10	-15.24	-12.74	-3.015
	PBE-D3/TZ	-13.78	-1.35	-11.44	-14.79	-3.82
	CCSD(T)/DZ	-15.01	-1.04	-9.34		
	SCS-MP2/DZ	-16.19	-0.97	-8.13	-11.86	-3.36
	SCS-MP2/TZ	-20.51	-1.02	-10.41	-12.26	-3.38
	DFT-SAPT/DZ	-13.48	-0.86	-7.33	-11.08	-3.25
	DFT-SAPT/TZ	-19.17	-0.97	-10.64	-11.42	-3.23
1c	BP+D3/TZ	-21.00	-0.51	-2.49	-30.06	-2.30
	PBE-D3/TZ	-16.04	-0.47	-3.23	-23.70	-2.98
	CCSD(T)/DZ	-15.27	-0.46	-2.47		
	SCS-MP2/DZ	-15.73	-0.465	-2.31	-23.51	-2.55
	SCS-MP2/TZ	-19.13	-0.47	-2.43	-25.12	-2.57
	DFT-SAPT/DZ	-13.05	-0.40	-2.01	-17.95	-2.45
	DFT-SAPT/TZ	-17.24	-0.43	-2.34	-19.92	-2.46

While with DZ basis sets SCS-MP2 agrees fairly well with the "gold standard" CCSD(T) method, i.e. within about 10%, the deviations of DFT-SAPT usually are larger (up to 20%). Though, as a rule of thumb and confirmed in table 2, the magnitude of interaction energies increases with increasing basis set size (here from DZ to TZ), this increase is expected to be different for supermolecular methods such as SCS-MP2 and CCSD(T) on the one hand and intermolecular perturbation theory such as DFT-SAPT on the other hand. Indeed, DFT-SAPT and SCS-MP2 tend to agree better with TZ basis sets – with the notable exception of the case of interactions between two naphthalene fragments. Here SCS-MP2 overestimates the magnitude of the π···π interaction energies by about 20% with respect to CCSD(T) as demonstrated by comparing the numbers presented in table 1 of ref [33]. Since essentially the same amount of

overestimation is also found comparing SCS-MP2 and DFT-SAPT (table 2) it can safely be assumed that DFT-SAPT reproduces the CCSD(T) level π···π interaction energy between the naphthalene subunits within a few percent. In summary, the SCS-MP2/TZ and DFT-SAPT/TZ interaction energies should certainly be regarded as the "best" sets of data in table 2, in the sense that they are presumably close to CCSD(T)/TZ interaction energies (which were not determined for reasons of computational expense), with SCS-MP2 yielding slightly more accurate interaction energies when one or two ds fragments are involved, and DFT-SAPT providing significantly more reliable np···np interaction energies. In view of this, BP+D3 clearly overestimates the magnitude of the π···π interactions, in the crystal structure fragments **1a** and **1c**, the CH···π interactions in **1a** and the Sb···Sb interactions in **1b**. Aside from a significant underestimation of the magnitude of the Sb···π interactions in **1b**, PBE+D3 overall is in better agreement with SCS-MP2 and DFT-SAPT. With PBE-D3 the interaction energies in the crystal structure fragments **1a**, **1b** and **1c** amount to -73.3, -34.7, and -42.3 kJ/mol, respectively, i.e. their magnitude in each case is about 23-24 kJ/mol lower than with BP+D3 (*vide supra*).

According to all employed quantum chemical methods **1a** is mainly stabilized by π···π interactions between the parallel naphthalene fragments and CH···π interactions between orthogonally arranged naphthalene fragments (last two columns in table 2). The interactions between the distibine and a diagonally neighbouring naphthalene fragment are also fairly significant for the dimer stability, whereas the remaining fragment-fragment interactions can be neglected.

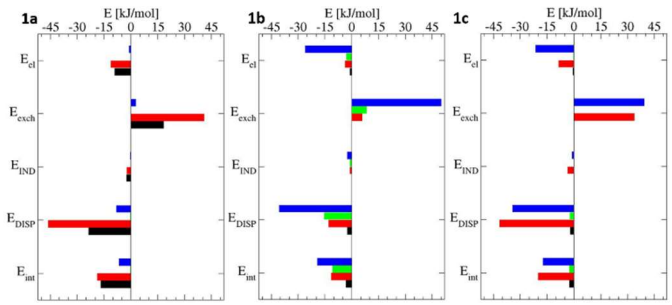

Figure 5. Energy contributions (Table S2) for the fragment-fragment interactions [ds···np (blue), ds···ds (green), np···np (red), np···np' (black)] in **1**.

The dispersion dominance of all fragment-fragment interactions in **1a** becomes evident in fig. 4, which shows the individual DFT-SAPT interaction contributions for the most relevant fragment pairs. The electrostatic energy, E_{el}, is a minor contributor to the total DFT-SAPT interaction energy, E_{int}, and the induction energy, E_{IND}, is nearly insignificant. Typical for classical *van der Waals* dimer, the dispersion energy, E_{DISP}, is the main stabilizing contribution, to some extent counterbalanced by the exchange-overlap energy (or steric repulsion), E_{exch}.

The ds···np' interactions in **1b** and **1c** are negligible and the np···np' interaction energies are fairly small (table 2), while the ds···np interaction is important. As might be expected from their spatial proximity the np···np interactions dominate in **1c**, which become reduced due to the parallel slide of both monomers in **1b**. In the latter, direct ds···ds interactions between the distibine fragments are significant. Figure 5 reveals that also in **1b** and **1c** most fragment-fragment interactions should be classified as *van der Waals* interactions, including the Sb···Sb interaction (ds···ds) in **1b**. The Sb···π (ds···np) interactions in **1b** and **1c** contain significant electrostatic contributions, as was observed for the $SbCl_3$···toluene complex.[34]

The importance of the Sb···π interactions for the stability of the crystal structure and the role of dispersion contribution, seconded by electrostatic attraction, to these interactions raise the question if this is similar for other pnictogen atoms. Hence we performed DFT+D calculations for structural motifs derived from fragment **1b** by replacing Sb with the respective pnictogen atom (P, As, Bi), followed by geometry optimization.[22-25] Employing BP+D3/TZ as for **1b'**, the results of the optimizations in all cases resemble the crystal structure fragment **1b** (the most important structural parameters are found in table S3). It should be noted that in the crystal structure of the P-analogue of **1** there is no structural motif which directly corresponds to **1b**, rather, there is a motif resembling **1c**. We thus performed an additional geometry optimization resulting in a dimer structure, which indeed corresponds to **1c**. As in the case of Sb, where **1c'** is more stable than **1b'**, i.e. by 5.2 kJ/mol, the P-analogue **1c'(P)** is more stable than **1b'(P)**, yet by a much larger margin, i.e. by 15.8 kJ/mol. Replacing BP+D3 with PBE+D3 we were not able to find a structural motif similar to **1b** for the P-analogue: starting from the structural motif **1b'(P)** as obtained from BP+D3, the PBE+D3 geometry optimization ended up in **1c'(P)**. Apparently, while **1b'(P)** is a local minimum structure at the BP+D3 level of theory, separated by a noticeable barrier from the deeper local minimum **1c'(P)**, this is no longer the case at the PBE+D3 level of theory. Similary, we were not able to obtain a structure **1b'(As)** from PBE+D3 geometry optimization, but rather directly **1c'(As)**. On the other hand, for the heavy pnictogen atoms (E=Sb, Bi) even on the PBE+D3 level of theory, both **1b'(E)** and **1c'(E)** were found to be stable local minima on the potential energy surface.

Table 3. Stabilization energies (in kJ/mol) of the BP+D3 and PBE+D3 optimized dimer structures of various pnictogen analogues of **1**.

		BP+D3	PBE+D3
P	1a'	-93.3	-68.3
	1b'	-55.5	---
	1c'	-71.3	-48.2
As	1a'	-96.0	-69.7
	1b'	-69.1	---
	1c'	-76.8	-50.4
Sb	1a'	-98.7	-71.1
	1b'	-64.4	-42.7
	1c'	-69.6	-47.2
Bi	1a'	-99.7	-71.3
	1b'	-79.1	-51.8
	1c'	-75.2	-50.3

The resulting stabilization energies are collected in table 3. Assuming that PBE+D3 stabilization energies are more reliable (*vide supra*) for the other pnictogen atoms as well, we observe an overestimation of the magnitude of the stabilization ener-

gies of 22-28 kJ/mol with BP+D3. Despite these findings, we opted for a fragment decomposition of the BP+D3 optimized dimer structures **1b'(P)**, **1b'(As)**, **1b'(Sb)**, and **1b'(Bi)**: though the first two entries in this list are most likely artefacts of the BP+D3 approach, this allows us to study the effect of changing the pnictogen atom in a consistent set of dimer structures. Table 4 contains the results of a fragment decomposition performed on hydrogen-capped fragments in a similar way as before (*cf.* table 2), but now for fragment structures constructed from BP+D3 optimized dimers (rather than crystal structure fragments).

Table 4. Fragment-fragment interaction energies (in kJ/mol) for BP+D3 optimized dimer structure of pnictogen analogues of **1**. TZ quality basis sets were used throughout.

		de···np	de···np'	de···de	np···np
1c'(P)	BP+D3	-21.80	-0.09	-0.73	-36.71
	PBE-D3	-18.33	-0.07	-1.16	-22.56
	SCS-MP2	-17.21	-0.07	-0.78	
	DFT-SAPT	-16.63	-0.041	-0.85	
1b'(P)	BP+D3	-18.95	-0.42	-6.56	-20.71
	PBE-D3	-11.85	-0.69	-7.77	-19.67
	SCS-MP2	-14.07	-0.44	-5.25	
	DFT-SAPT	-12.68	-0.42	-5.83	
1b'(As)	BP+D3	-25.26	-0.70	-8.75	-19.34
	PBE-D3	-15.31	-0.88	-8.39	-18.96
	SCS-MP2	-17.12	-0.64	-5.92	
	DFT-SAPT	-15.83	-0.61	-6.11	
1b'(Sb)	BP+D3	-23.40	-0.92	-11.05	-14.47
	PBE-D3	-17.06	-1.01	-9.62	-16.08
	SCS-MP2	-23.98	-0.88	-8.13	
	DFT-SAPT	-22.05	-0.83	-7.93	
1b'(Bi)	BP+D3	-27.97	-1.20	-18.31	-12.55
	PBE-D3	-19.77	-1.26	-14.12	-14.77
	SCS-MP2	-28.19	-1.15	-12.79	
	DFT-SAPT	-24.95	-1.08	-11.96	

As expected, de···np' interactions are hardly relevant for the considered dimers. np···np interactions, on the other hand, are relevant and even play a dominant role in the stabilization of **1c'(P)**, similar to the case of **1c(Sb)** discussed above. In **1b'(E)** the size of the np···np interactions changes only indirectly as a consequence of structural changes imposed by the various pnictogen atoms. We thus concentrate on the de···np and de···de fragment interactions of **1b'(E)**. BP+D3 and PBE+D3 differ here significantly, the latter showing much smaller magnitudes of the interaction energies for de···np, while they agree fairly well for de···de with exception of **1b'(Bi)** (for a graphical representation see Figure S6). Both DFT+D sets of data deviate notably from the SCS-MP2 and DFT-SAPT results. SCS-MP2 and DFT-SAPT, on the other hand, agree within about 10%, the largest absolute deviations here are observed for **1b'(Bi)** with 3.2 and 0.8 kJ/mol for de···np and de···de, respectively. In view of the totally different theoretical foundations of both approaches we take this as an indication for the reliability of the obtained fragment-fragment interaction energies. Both methods clearly demonstrate a monotonous increase of the size of the interaction energy for de···np and de···de with the nuclear charge of the pnictogen atom, which for de···np is nearly linear. Both, the de···np and de···de interaction energies, approximately double upon replacing P with Bi.

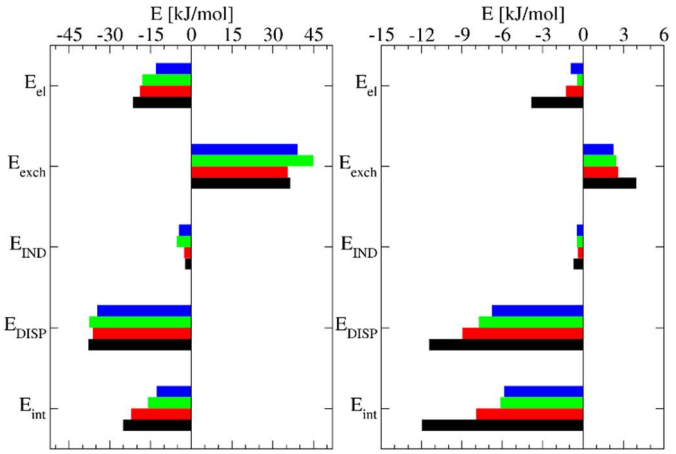

Figure 6. Energy contributions (Table S4) for the fragment-fragment interactions de···np (left) and de···de (right) for the pnictogen analogues of **1** (P: blue; As: green; Sb: red and Bi: black).

Figure 6, which shows the individual SAPT contributions to these interaction energies, makes clear that the increase of E_{int} is mainly due to the increase in the dispersion energy for the pnictogen-pnictogen interactions, while a combination of the electrostatic, exchange and dispersion contributions is responsible in case of pnictogen-π interactions. One should note that the stabilization energies for **1b'(E)** do not show the same strong increase as the de···np and de···de fragment interaction energies along the series E= P, As, Sb and Bi (*cf.* table 3) due to a partial cancellation with decreasing np···np interaction energies resulting from increasing distances between the neighbouring naphthyl groups (*cf.* table S4).

Conclusions

The molecular structure of $Naph_2Sb_2$ **1** is comparable to that of the phosphorous analogue $Naph_2P_2$ and other diphosphines containing comparable rigid backbones, whereas the packing of the molecules within the crystal structures of **1** and $Naph_2P_2$ slightly differs. The most important building block (structural motif Figures 3a/4a) in both compounds can be described as brick-like and is characterised by relatively strong, classical dispersion-dominated CH···π and π···π interactions between the naphthyl ligands according to quantum chemical calculations. In addition, **1** and $Naph_2P_2$ both show π···π interactions between naphthyl units connecting neighbouring bricks (Figures 3c/4c). In contrast, **1** exhibits Sb···π (ds···np) interactions (Figure 3c), whereas similar P···π (dp···np) interactions were not observed in the crystal structure of $Naph_2P_2$. Quantum chemical calculations proved that the Sb···π interactions are much stronger than the comparable P···π interactions, and the same is true for the Sb···Sb interactions (structural motif in Figure 3b) as compared to the hypothetical P···P interactions. The calculated E···E interactions between all pnictogen atoms (E = P, As, Sb, Bi) were found to by dispersion dominated, while the E···π interactions additionally contained significant

electrostatic attraction. The resulting total magnitudes of the fragment-fragment interaction energies were found to strongly grow with increasing atomic number of the pnictogen atom. These findings in combination with the impossibility to optimise a structural motif as depicted in Figure 3b for $Naph_2P_2$ and $Naph_2As_2$ at the PBE+D3 level of theory, leads us to speculate that the hitherto unknown crystal structure of $Naph_2As_2$ will be similar to that of $Naph_2P_2$, whereas $Naph_2Bi_2$ should rather adopt a structure as determined for $Naph_2Sb_2$.

Experimental

All manipulations were performed in an atmosphere of purified argon using standard Schlenk and glove-box techniques. Chloroform and F-benzene were carefully dried over CaH_2 whereas tetrahydrofuran was distilled over Na/benzophenone ketyl. $CDCl_3$ was dried over activated molecular sieves (4 Å) and degassed prior to use. The anhydrous nature of the solvents was verified by Karl Fischer titration. $Li_2Naph{\cdot}TMEDA$[35] was prepared according to literature methods and other chemicals were obtained from commercial sources and purified prior to use. The ^1H (300 MHz) and $^{13}C\{^1H\}$ (150 MHz) NMR (δ in ppm) spectra were recorded using a Bruker Avance DPX-300 or Bruker Avance III HD spectrometers and the spectra were referenced to internal $CDCl_3$ (^1H: δ = 7.240; ^{13}C: δ = 77.230). The microanalysis was performed at the elemental analysis laboratory of University of Duisburg-Essen. The IR spectrum of **1** was recorded with an ALPHA-T FT-IR spectrometer equipped with a single reflection ATR sampling module. The IR spectrometer was placed in a glovebox to guarantee measurements under inert gas conditions. The melting point was measured using a Thermo Scientific 9300 apparatus

Synthesis of 2: A solution of $SbCl_3$ (196 mg, 0.858 mmol) in 5 mL of THF was added dropwise to a solution of $Li_2Naph{\cdot}TMEDA$ (330 mg, 1.288 mmol) in 5 mL of THF at -78 °C. The reaction mixture was slowly warmed to room temperature and stirred at this temperature for additional 30 minutes. After removing all volatiles under reduced pressure, the resulting yellow residue was extracted with 15 mL of fluorobenzene. The solvent was removed in vacuum and the resulting solid residue dissolved in 5 mL of $CHCl_3$ and stored at -30°C to yield **1**. Single crystals of **1** were obtained after re-crystallisation in $CHCl_3$ at 0°C. Yield: 102 mg (0.206 mmol, 48%). M.p.: 219 °C. Anal. Calcd. for $C_{20}H_{12}Sb_2$: C, 48.45; H, 2.44. Found: C, 48.39; H, 2.48%. IR (neat): ν 3037, 2959, 2929, 1483, 1435, 1345, 1261, 1195, 1093, 1015, 967, 805, 769, 432 cm-1. ^1H NMR (C_6D_6, 300.1 MHz, 25 °C): δ 8.03 (d, $^3J_{HH}$ = 6.6 Hz, 4 H, 4,5-Naph-H), 7.55 (d, $^3J_{HH}$ = 8.1 Hz, 4 H, 2,7-Naph-H), 7.34 (t, $^3J_{HH}$ = 8.1 Hz, 4 H, 3,6-Naph-H). 13C NMR (C_6D_6, 150 MHz, 25 °C): δ 147.3 (10-Naph-C), 146.6 (9-Naph-C), 138.0 (2,7-Naph-C), 137.5 (1,8-Naph-C), 128.7 (4,5-Naph-C), 126.5 (3,6-Naph-C).

Single crystal X-ray diffraction. Crystallographic data of **1**, which were collected on a Bruker D8 Kappa APEX2 diffractometer (mono-chromated MoK_α radiation, λ = 0.71073 Å) at 100(1) K, are summarized in Table S1. The crystal of **1** was mounted on a nylon loop in inert oil. The solid-state structure of **1** is shown in Figures 1, while figure 2 displays a 3D packing plot of **1**. The structure was solved by Direct Methods (SHELXS-97)[36] and refined anisotropically by full-matrix least-squares on F2 (SHELXL-2014).[37,38] Absorption corrections were performed semi-empirically from equivalent reflections on basis of multi-scans (Bruker AXS APEX2). Hydrogen atoms were refined using a riding model. The highest residual peak is 0.66 Å away from Sb1 and a result of either Fourier truncation effects or residual absorption errors.

CCDC-1537302 contains the supplementary crystallographic data for this paper. These data can be obtained free of charge from The Cambridge Crystallographic Data Centre via www.ccdc.cam.ac.uk/data_request/cif.

Quantum chemical calculatations. Details of the quantum chemical calculations are given in the supporting information file.

Acknowledgements

St.S. and G.J. acknowledge financial support of the work by the DFG within the priority program SPP 1807 (projects SCHU 1069/19-1; JA954/4-1).

Notes and references

1 For a historical review see: D. Seyferth, *Organometallics*, 2001, **20**, 1488.
2 F. A. Paneth, *Trans. Faraday Soc*., 1934, **30**, 179; F. A. Paneth and H. Loleit, *J. Chem. Soc*., 1935, 366.
3 C. Silvestru, H. J. Breunig and H. Althaus, *Chem. Rev*., 1999, **99**, 3277; H. J. Breunig and R. Rössler, *Chem. Soc. Rev*., 2000, **29**, 403; L. Balázs and H. J. Breunig, *Coord. Chem. Rev*., 2004, **248**, 603; H. J. Breunig, *Z. Anorg. Allg. Chem*., 2005, **631**, 621.
4 A. J. Ashe, III, W. Butler and T. R. Diephouse, *J. Am. Chem. Soc*. 1981, **103**, 207; A. J. Ashe, III, E. G. Ludwig, Jr. and J. Oleksyszyn, *Organometallics* 1983, **2**, 1859; A. J. Ashe, III, E. G. Ludwig, Jr., J. Oleksyszyn and J. C. Huffman, *Organometallics*, 1984, **3**, 337; S. Roller, M. Dräger, H. J. Breunig, M. Ates and Gülec, S. *J. Organomet. Chem*., 1987, **329**, 319; O. Mundt, H. Riffel, G. Becker and A. Simon, *Z. Naturforsch. B*, 1988, **43**, 952; G.; Becker, M. Meiser, O. Mundt and J. Weidlein, *Z. Anorg. Allg. Chem*., 1989, **569**, 62; S. Roller, M. Dräger, H. J. Breunig, M. Ates and S. Gülec, *J. Organomet. Chem*., 1989, **378**, 327.
5 T. Hughbanks, R. Hoffmann, M.-H. Whangbo, K. R. Stewart, O. Eisenstein and E. Canadell, *J. Am. Chem. Soc*., 1982, **104**, 3816; A. J. Ashe, III, J. W. Kampf and D. B. Puranik, *Organometallics*, 1992, **11**, 2743; L. L. Lohr and A. J. Ashe III, *Organometallics*, 1993, **12**, 343; G. Balázs, H. J. Breunig, E. Lork and W. Offermann, *Organometallics*, 2001, **20**, 2666; G. Balázs, H. J. Breunig and E. Lork, *Organometallics*, 2002, **21**, 2584; L. Balázs, H. J. Breunig, E. Lork, C. Silvestru, *Eur. J. Inorg. Chem*., 2003, 1361; L. Balázs, H. J. Breunig and E. Lork, *Z. Naturforsch. B*, 2005, **60**, 180; L. Balázs, H. J. Breunig, C. Silvestru and R. Varga, *Z. Naturforsch. B*, 2005, **60**, 1321; L. Balázs, H. J. Breunig, E. Lork, A. Soran and C. Silvestru, *Inorg. Chem*., 2006, **45**, 2341; R. Wolf, J. Fischer, R. C. Fischer, J. C. Fettinger and P. P. Power, *Eur. J. Inorg. Chem*., 2008, 2515; H. J. Breunig, E. Lork, O. Moldovan and C. I. Rat,, *J. Organomet. Chem*., 2008, **693**, 2527; L. Dostál, R. Jambor, A. Růžička and P. Šimon, *Eur. J. Inorg. Chem*., 2011, 2380; S. Shimada, J. Maruyama, Y.-K. Choe and T. Yamashita, *Chem. Commun*., 2009, 6168; K. Y. Monakhov, T. Zessin and G. Linti, *Eur. J. Inorg. Chem*., 2010, 322.

6 A. G. M. Barrett and L. M. Melcher, *J. Am. Chem. Soc*., 1991, **113**, 8177.
7 S. Ishida, F. Hirakawa, K. Furukawa, K. Yoza and T. Iwamoto, *Angew. Chem*., 2014, **126**, 11354; *Angew. Chem. Int. Ed*., 2014, **53**, 11172; R. J. Schwamm, J. R. Harmer, M. Lein, C. M. Fitchett, S. Granville and M. P. Coles, *Angew. Chem*., 2015, **127**, 10776; *Angew. Chem. Int. Ed*., 2015, **54**, 10630.
8 a) A. Kuczkowski, S. Heimann, A. Weber, S. Schulz, D.; Bläser and C. Wölper, *Organometallics*, 2011*,* **30***,* 4730; b) S. Schulz, S. Heimann, A. Kuczkowski, C. Wölper and D. Bläser, *Organometallics*, 2013, **32**, 3391.
9 A. Kuczkowski, S. Fahrenholz, S. Schulz, M. Nieger and P. Saarenketo, *Organometallics*, 2001, **20**, 2000; A. Kuczkowski, S. Schulz and M. Nieger, *Angew. Chem*., 2001, **113**, 4351; *Angew. Chem. Int. Ed*., 2001, **40**, 4222; A. Kuczkowski, S. Fahrenholz, S. Schulz and M. Nieger, *Organometallics*, 2004, **23**, 3615; D. Schuchmann, A. Kuczkowski, S. Fahrenholz, S. Schulz and U. Flörke, *Eur. J. Inorg. Chem*., 2007, 931;S. Heimann, S. Schulz, D. Bläser and C. Wölper, *Eur. J. Inorg. Chem*., 2013, **28**, 4909; S. Heimann, A. Kuczkowski, D. Bläser, C. Wölper, R. Haack, G. Jansen and S. Schulz, *Eur. J. Inorg. Chem*., 2014, **28**, 4858, S. Heimann, D. Bläser, C. Wölper and S. Schulz, *Organometallics*, 2014, **33**, 2295; C. Ganesamoorthy, D. Bläser, C. Wölper and S. Schulz, *Angew. Chem*., 2014, **126**, 11771; *Angew. Chem. Int. Ed*., 2014, **53**, 11587.
10 A. Karacar, H. Thonnessen, P. G. Jones, R. Bartsch and R. Schmutzler, *Chem. Ber./Recueil*, 1997, **130**, 1485; A. Karacar, M. Freytag, P. G. Jones, R. Bartsch and R. Schmutzler, *Z. Anorg. Allg. Chem*., 2001, **627**, 1571; A. Karacar, M. Freytag, H. Thonnessen, P. G. Jones, R. Bartsch and R. Schmutzler, *J. Organomet. Chem*., 2002, **643–644**, 68; P. Kilian, A. M. Z. Slawin and J. D. Woollins, *Chem. Eur. J*., 2003, **9**, 215; K. Owsianik, L. Vendier, J. Błaszczyk, L. Sieroń, *Tetrahedron*, 2013, **69**, 1628.
11 M. Jura, W. Levason, G. Reid and M. Webster, *Dalton Trans*., 2008, 5774.
12 S. M. Aucott, H. L. Milton, S. D. Robertson, A. M. Z. Slawin and J. D. Woollins, *Heteroatom Chem*., 2004, **15**, 530; F. R. Knight, A. L. Fuller, M. Bühl, A. M. Z. Slawin and J. D. Woollins, *Chem. Eur. J*., 2010, **16**, 7605; F. R. Knight, A. L. Fuller, M. Bühl, A. M. Z. Slawin and J. D. Woollins, *Chem. Eur. J*., 2010, **16**, 7503
13 F. R. Knight, A. L. Fuller, M. Bühl, A. M. Z. Slawin and J. D. Woollins, *Chem. Eur. J*., 2010, **16**, 7617
14 For review articles see: P. Kilian, F. R. Knight and J. D. Woollins, *Chem. Eur. J*., 2011, ***17***, 2302; P. Kilian, F. R. Knight and J. D. Woollins, *Coord. Chem. Rev*., 2011, **255**, 1387.
15 Crystallographic data of **1** are given in the supporting information file.
16 32 entries were found in the CSD version 5.38 (update Nov. 2016); the Sb-Sb bond length range from 2.644 - 3.030 Å (mean 2.86(6) Å).
17 M. Zhao, L. Wang, X. Zhanga and W. Zheng, *Dalton Trans*., 2016, **45**, 10505; A. Hinz, J. Rothe, A. Schulz and A. Villinger, *Dalton Trans*., 2016, **45**, 6044.
18 M. Baba and T. Mizuta, *Polyhedron*, 2015, **92**, 30.
19 N. A. Piro, J. S. Figueroa, J. T. McKellar and C. C. Cummins, *Science*, 2006, **313**, 1276.
20 D. Tofan and C. C. Cummins, *Angew. Chem*., 2010, **122**, 7678; *Angew. Chem. Int. Ed*., 2010, **49**, 7516.
21 F. Furche, R. Ahlrichs, C. Hättig, W. Klopper, M. Sierka and F. Weigend, *WIREs Comput. Mol. Sci.*, 2014, **4**, 91.; H.-J. Werner, P. J. Knowles, G. Knizia, F. R. Manby and M. Schütz, *WIREs Comput. Mol. Sci.*, 2012, **2**, 242.
22 A. D. Becke, *Phys. Rev. A* 1988, **38**, 3098; J. P. Perdew, *Phys. Rev. B* 1986, **33**, 8822.
23 S. Grimme, J. Antony, S. Ehrlich and H. Krieg, *J. Chem. Phys.* 2010, **132**, 154104.
24 F. Weigend and R. Ahlrichs, *Phys. Chem. Chem. Phys.* 2005, **7**, 3297; F. Weigend, *Phys. Chem. Chem. Phys.* 2006, **8**, 1057.
25 For full technical details see supplementary information.
26 Determined from BP+D3/def2-TZVP geometry optimization of SbH_3.
27 *CRC Handbook of Chemistry and Physics*, 64th Edition, R. C. Weast, M. J. Astle, W. H. Beyer (Eds.) CRC Press, Boca Raton, 1984.
28 A) J.P. Perdew, K. Burke and M. Ernzerhof, *Phys. Rev. Lett*., 1996, **77**, 3865. b) J.P. Perdew, K. Burke and M. Ernzerhof, *Phys. Rev. Lett*., 1997, **78**, 3865.
29 S. F. Boys and F. Bernardi, *Mol. Phys*., 1970, **19**, 553.
30 S. Grimme, *J. Chem. Phys.*, 2003, **118**, 9095.
31 G. Jansen, *WIREs Comput. Mol. Sci.*, 2013, **4**, 127.; B. Jeziorski, R. Moszynsky and K. Szalewicz, *Chem. Rev.,* 1994, **94**, 1887.; K. Szalewicz, , *WIREs Comput. Mol. Sci.*, 2012, **2**, 254.
32 R. A. Kendall, T. H. Dunning and R. J. Harrison, *J. Chem. Phys.*, 1992, **96**, 6796.
33 T. Janowski and P. Pulay, *J. Am. Chem. Soc*., 2012, **134**, 17520.
34 R. Lo, P. Švec, Z. Růžičková, A. Růžička and P. Hobza, *Chem. Commun.*, 2016, **52**, 3500.
35 J. van Soolingen, R.-J. de Lang, R. den Besten, P. A. A. Klusener, N. Veldman, A. L. Spek and L. Brandsma, *Syn. Commun*., 1995, **25**, 1741.
36 G. M. Sheldrick, *Acta Crystallogr*., 1990, **A46**, 467.
37 G. M. Sheldrick, SHELXL-2014, Program for the Refinement of Crystal Structures University of Göttingen, Göttingen (Germany) 2014. (see also: G. M. Sheldrick, *Acta Crystallogr*. 2008, **A64**, 112).
38 shelXle, A Qt GUI for SHELXL, C. B. Hübschle, G. M. Sheldrick and B. Dittrich, *J. Appl. Cryst*., 2011, **44**, 1281.

DOI: 10.1039/C7DT02165H
URN: urn:nbn:de:hbz:464-20201210-175036-4

Accepted Manuscript. The final article was published in: Dalton Trans., 2017,46, 9227-9234 and is available at: https://doi.org/10.1039/C7DT02165H